PCCP

Temperature effects on the spatial distribution of electrolyte mixtures at the aqueous liquid-vapor interface

Journal:	*Physical Chemistry Chemical Physics*
Manuscript ID	CP-ART-12-2019-006729.R1
Article Type:	Paper
Date Submitted by the Author:	17-Mar-2020
Complete List of Authors:	Eggimann, Becky; Wheaton College, Department of Chemistry Siepmann, Joern Ilja; University of Minnesota, Dept of Chemistry

PCCP

ARTICLE TYPE

Cite this: DOI: 00.0000/xxxxxxxxxx

Temperature effects on the spatial distribution of electrolyte mixtures at the aqueous liquid-vapor interface†

Becky L. Eggimann,*[a] and J. Ilja Siepmann*[bc]

Received Date
Accepted Date

DOI: 00.0000/xxxxxxxxxx

The microscopic picture of ions at the aqueous liquid-vapor interface continues to be an important and active area of research. Both experiments and simulations have shown that certain ions, such as Br^- and I^-, prefer to adsorb at the interface, but there is not yet a consensus as to the relative importance of various ion-specific properties that influence surface solvation. In a previous study, we systematically explored the effect of ion size on determining whether or not a monovalent ion would adsorb at the surface, and found that, for electrolyte mixtures represented by non-polarizable models, the larger/smaller anions are enriched/depleted at the interface. Here, we extend that study to include temperature effects enabling a van't Hoff analysis of the enthalpic and entropic contributions. We perform configurational-bias Monte Carlo simulations in the Gibbs ensemble to investigate the partitioning of mixtures of differently sized ions at the aqueous liquid-vapor interface from 284.09 K to 347.22 K at a pressure of 1 atm. Ions are represented using our own previously developed models that vary only in size (i.e., the Lennard-Jones σ parameter changes, while all other parameters are held constant across ion types). System properties studied include surface tension, interfacial width, ion surface excess, number density profiles, z-dependent transfer free energy, enthalpy, entropy, and anion-cation coordination numbers.

1 Introduction

Certain large, polarizable anions are preferentially solvated at the air-water interface. This is the view that has emerged as the consensus of both experiment and theory, overturning the long held view to the contrary.[1,2] Because aqueous halide solutions, including the large, polarizable anions Br^- and I^-, exhibit increased surface tension relative to pure liquid water, thermodynamic reasoning suggests that ions should be (partially) excluded from the air-water interface. The favorable interactions between halide ions and water stabilize the bulk region relative to the surface and the amount of surface tension increase could be attributed to the exclusion of ions from the surface by image charge repulsion.[3] Nevertheless, numerous studies (see, for example, reviews in 2006[1], 2012[4], and 2013[2]) probing the aqueous liquid-vapor interface with molecular-level detail have collectively demonstrated that surface solvation can occur, and is a requirement for certain atmospheric chemical reactions.[5] The ability to explain and predict with accuracy the molecular behavior of such important interfaces as atmospheric aerosols and the natural gas-water and protein-water interfaces (which are notably similar, though more complex, hydrophobe-water interfaces) requires that we better understand the connection between the thermodynamics of ion solvation and the microscopic spatial distribution preferences of these ions. This has prompted further exploration of the molecular driving forces and solute-specific properties that might give rise to the unexpected spatial distributions observed.

Fundamentally, ions (or other solutes) will preferentially adsorb to the air-water interface when there is a favorable balance of transfer enthalpy and transfer entropy, leading to a transfer free energy minimum at the surface. Note that thermodynamic equilibrium requires that an ion's chemical potential is equal regardless of spatial location in the system. Contributions to the transfer enthalpy can come from the water-water and water-ion interactions, while entropy must be sacrificed to form a cavity in the bulk solution to hold the ion. Some of the first evidence for surface adsorption of ions came from molecular simulations of water clusters that employed polarizable models.[6–8] Even more complex descriptions of the interactions including force fields allowing for charge transfer (in addition to polarizability) and Kohn-Sham density functional theory also support a propensity of large halide ions for the interface.[9–12] Molecular simulations, which allow precise control of model properties, are well suited to teasing out the relative contributions to the overall free energy. The special ability of polarizable ions to adapt to the surface by creating an asymmetric charge distribution that maximizes the

[a] Department of Chemistry, Wheaton College, Wheaton, IL, 60187 USA. E-mail: becky.eggimann@wheaton.edu
[b] Department of Chemistry and Chemical Theory Center, University of Minnesota, Minneapolis, MN, 55455 USA. E-mail: siepmann@umn.edu
[c] Department of Chemical Engineering and Materials Science, University of Minnesota, Minneapolis, MN, 55455 USA.

ion-water interaction seemed to be a necessary condition and likely driving force for surface solvation.[8,13] Further work, including a previous study of our own, demonstrated that polarizability was not absolutely necessary.[14–18] Our work involved simulations of ion mixtures of different sizes and used Gibbs ensemble Monte Carlo simulations to show that large anions will distribute preferentially into the interface, even for fixed-charge models.[17] Noah-Vanhoucke and Geissler also demonstrated that by carefully controlling the size and charge of an ion, they could make a fixed-charged ion distribute into either the bulk or the surface as desired.[15] This suggested that polarizability, while helpful, is not a necessary condition for surface adsorption. As long as the strength of the ion-water interaction–higher charges will make bulk solvation more favorable–is balanced against the entropic penalty for cavity formation–larger sizes will make bulk solvation less favorable–surface solvation can occur.

Given the molecular complexity of these interfaces and the challenges of modeling real ions, questions remain regarding the role of solute-specific properties and the particular interactions that impact the overall entropy/enthalpy balance at interfaces.[19,20] Caleman et al. performed potential of mean force calculations using polarizable models to determine the free energy profiles for moving a single halide ion from the interior to the surface of a water droplet.[21] They showed that the free energy minimum at the surface was dominated by favorable enthalpy–a surprise given that the ion-water interaction would be maximized in the bulk where a full solvation shell could be formed, rather than the surface where the ion is only partially hydrated. By looking at the contributions to the enthalpy coming from the water-water interactions and the ion-water interactions, they found that the ion-water interactions are indeed less favorable at the surface but that the favorable water-water interactions significantly increase as the ion is excluded. It is this recovery of water-water interactions that dominates the free energy profile. Entropy, again somewhat surprisingly, was shown to be a smaller contributor and even unfavorable when the ion was at the interface. Thus, the conclusion of Caleman et al. was that the entropic penalty of cavity formation was not a significant factor. Rather, the unfavorable entropy at the interface was explained by the decrease in surface fluctuations as the ion entered the region (i.e., "pinning" of capillary waves).[21] Otten et al. noted similar results for simulations with fixed-charge ion and water models that had been tuned for surface solvation of the ion, as well as for second harmonic generation experiments with thiocyanate solutions.[22] In both cases, they observed a favorable enthalpy and a smaller, unfavorable entropy in the surface region ($\Delta H = -11.8 \pm 0.8$ kJ/mol and $\Delta S = -17 \pm 3$ J/K mol for SCN^-).[22] This result–negative enthalpy and smaller, negative entropy at the surface–appears to be a general conclusion for ions that exhibit a preference for the air-water interface, though the proposed explanations, particularly the role of surface fluctuations and of direct ion-water versus indirect (solute-induced) water-water interactions, continue to be disputed.[11,23–29]

Whether or not this general conclusion holds in more complicated systems, i.e., systems that contain more than a single anion type, is an open question. The behavior of ions in mixed salt solutions has not yet been studied in great detail, despite that the atmospherically relevant solution, sea water, is a complex mixture of several ions. Simulations of NaCl and NaBr mixtures have shown that, at least at high concentrations, Cl^- can enhance the presence of Br^- at the air-water interface above that observed for pure NaBr solutions.[30] In our own earlier study, we also found that large anions that by themselves would have a surface preference can be excluded from the interface when mixed with even larger, more surface active anions.[17] Thus, competition between ions with different individual propensities for the surface makes it difficult to extrapolate the results of single salt solutions to more complex mixtures.

In an effort to further explore these mixture effects and determine the underlying entropy/enthalpy balance for ions with a range of spatial distributions, we perform Gibbs-ensemble Monte Carlo simulations of aqueous salt solutions that contain a mixture of differently-sized ions over a range of temperatures, from 284.09 K to 347.22 K. The ion mixtures are similar to those used in previous work,[17] but the extended temperature range allows for additional analysis. Specifically we are interested in the van't Hoff relationship between temperature and the Gibbs free energy of transfer for moving an ion from the bulk liquid into the interface. From this analysis (assuming negligible heat capacity effects[31]) we can obtain the separate contributions from enthalpy and entropy in governing the spatial distribution of ions in a mixture relative to both the air-water interface and the other ions.

2 Simulation Details

Because the current project is an extension of previous work, the aqueous vapor-liquid interface is modeled using similar rigid, fixed-charge force fields.[17] The system is a mixed salt solution composed of 2122 molecules of TIP4P[32] water, a mixture of five differently-sized anions, 10 of each size, and 50 oppositely-charged cations for system neutrality. The total solution contains 2222 particles. Compared to our previous work, the number of anion types is reduced from 9 to 5, while the number for each size is increased from 4 to 10 (and the number of water molecules is increased from 1528 to 2122 to maintain the same total ion concentration) to aid gathering sufficient precision for the van't Hoff analysis. Interactions between particles are comprised of pairwise-additive Lennard-Jones (LJ) and Coulomb potentials. For all ions, the LJ well-depth (ε) is fixed at 50.3 k_BK (i.e., equal to a value of 0.1 kcal/mol)[17] and charges are ± 1 |e|. The five unique anion models have LJ diameters (σ) of 4.1, 4.6, 5.1, 5.7, and 6.4 Å, which is an approximately 40% expansion of the ion volume with each step up in size. Cations share the same ε as the anions, and σ fixed at 3.3 Å. A spherical potential truncation is applied to the LJ interactions ($r_{cut} = 15$ Å) and the Ewald summation technique (with convergence parameter, κ, set to $3.3/r_{cut}$) is used to calculate the Coulomb interactions. Representative snapshots of the system at two different temperatures are shown in Figure 1.

Anticipating the eventual van't Hoff analysis, the simulations are performed at five different temperatures ranging from 284.09 K to 347.22 K in linear increments of $1/T = 0.00016$ (see Table 1). The algorithm of choice is configurational-bias Monte Carlo in

Table 1 Average boxlengths, number of particles, and vapor pressures for electrolyte mixtures at five different temperatures

		Vapor Box				Interfacial Box		
T [K]	$1000/T$ [K^{-1}]	L_{vap} [Å]	N_{vap}^{He}	N_{vap}^{water}	P_{vap} [kPa]	L_z [Å]	N_{int}^{He}	N_{int}^{water}
284.09	3.52	186.1 ± 0.2	162.7 ± 0.2	3.3 ± 0.3	101.5 ± 0.3	180 ± 10	2.3 ± 0.2	2118.7 ± 0.3
297.62	3.36	161.2 ± 0.3	97.9 ± 0.2	4.9 ± 0.5	101.6 ± 0.4	174 ± 8	2.1 ± 0.2	2117.1 ± 0.5
312.50	3.20	141.1 ± 0.6	58.28 ± 0.14	7.3 ± 0.6	101.6 ± 0.7	170 ± 8	1.72 ± 0.14	2114.7 ± 0.6
328.95	3.04	119.5 ± 0.9	28.68 ± 0.14	9.2 ± 0.6	101.8 ± 1.3	165 ± 9	1.32 ± 0.14	2112.8 ± 0.6
347.22	2.88	126 ± 2	19.25 ± 0.08	23 ± 2	101.7 ± 1.0	163 ± 9	0.75 ± 0.08	2099 ± 2

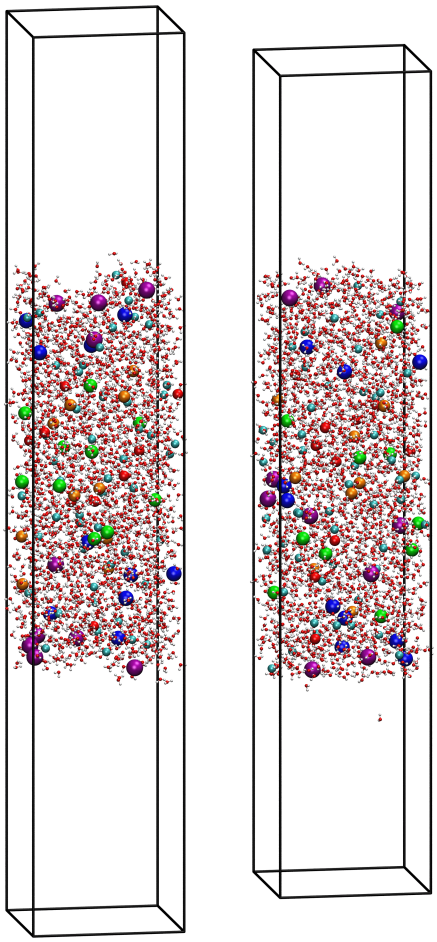

Fig. 1 System snapshots at 284.09 K (left) and 347.22 K (right). Water molecules are represented as ball-and-stick models with oxygen and hydrogen atoms shown in red and gray, respectively. Ions are represented with differently-sized spheres from smallest to largest: positively-charged counterion (cyan; $\sigma = 3.3$ Å), anion A (red; $\sigma = 4.1$ Å), anion B (orange; $\sigma = 4.6$ Å), anion C (green; $\sigma = 5.1$ Å), anion D (blue; $\sigma = 5.7$ Å), anion E (purple; $\sigma = 6.4$ Å).

the NpT-Gibbs ensemble[33–37]. As in previous work, the two-box NpT version of the Gibbs ensemble is preferred to a single-box interfacial system because the external pressure can be specified at 1 atm, resulting in a better match to experimental conditions. In the two-box set up, one box elongated along the z-direction contains the electrolyte solution in a slab configuration with fixed interfacial area surrounded by a vapor region. The other, the bulk vapor phase, is a cubic box that contains mostly helium atoms. The liquid slab consists of water and ions and has dimensions of 30 Å $\times$ 30 Å $\times \approx 77$ Å, separated by at least 80 Å of vapor from its periodic images in the z-direction. The cubic vapor box contains a mixture of helium atoms and some water molecules. For each temperature, the number of helium atoms is adjusted so that the vapor box contains less than 25 water molecules on average. This helps to keep the liquid slabs similarly sized across all temperatures (see Table 1).

During the simulation, all particles are allowed to translate, while for water, the only multi-atom molecule in the system, additional rotation moves are applied. The pressure of the vapor phase is maintained at the specified value (1 atm) by allowing volume moves in all dimensions of the vapor box and only in the z-dimension of the interfacial box (i.e., the interfacial area remains constant). Water molecules and helium atoms are allowed to swap between the two boxes so that the chemical potentials equilibrate and the vapor region surrounding the liquid slab exerts the externally specified pressure. Special "identity switch" moves are used to efficiently sample the spatial positions of the anions. This move type allows an anion to exchange position with any anion one size above or below itself. Optimization of the switch rates leads to efficient sampling and prevents any particular switch from happening more frequently than the others.

A total of 32 independent starting configurations are used for each temperature. Equilibration consists of more than 150000 cycles (one cycle consists of $N = 2222$ randomly selected moves), followed by more than 500000 cycles for production. Average properties for each temperature are calculated inclusively over all 32 independent simulations. Statistical uncertainties are reported as the standard error of the mean.

3 Results and Discussion

3.1 Density Profiles

In the equilibrated systems, the preferred positions of the ions relative to the surface of the liquid-water slab are determined by looking at the ion density as a function of z-position within the slab (see Figure 2). The number density profile for the solvent (i.e., water) determines the surface location and can be fit with a hyperbolic tangent function (Equation 1) to find the Gibbs dividing surface (GDS) and interfacial width:

$$\rho(z) = \frac{(\rho_{liq} + \rho_{gas})}{2}\left[1 - \tanh\left(\frac{z - z_0}{\xi}\right)\right] \quad (1)$$

Here ρ_{liq} and ρ_{vap} are the average densities of water in the interior regions of the liquid and vapor sections of the interfacial box (i.e., not including the mass density from the ions), where the latter can also be obtained with more precision from the vapor box. Since the liquid region can move throughout the simulation trajectory, z is the distance relative to the center of mass of the

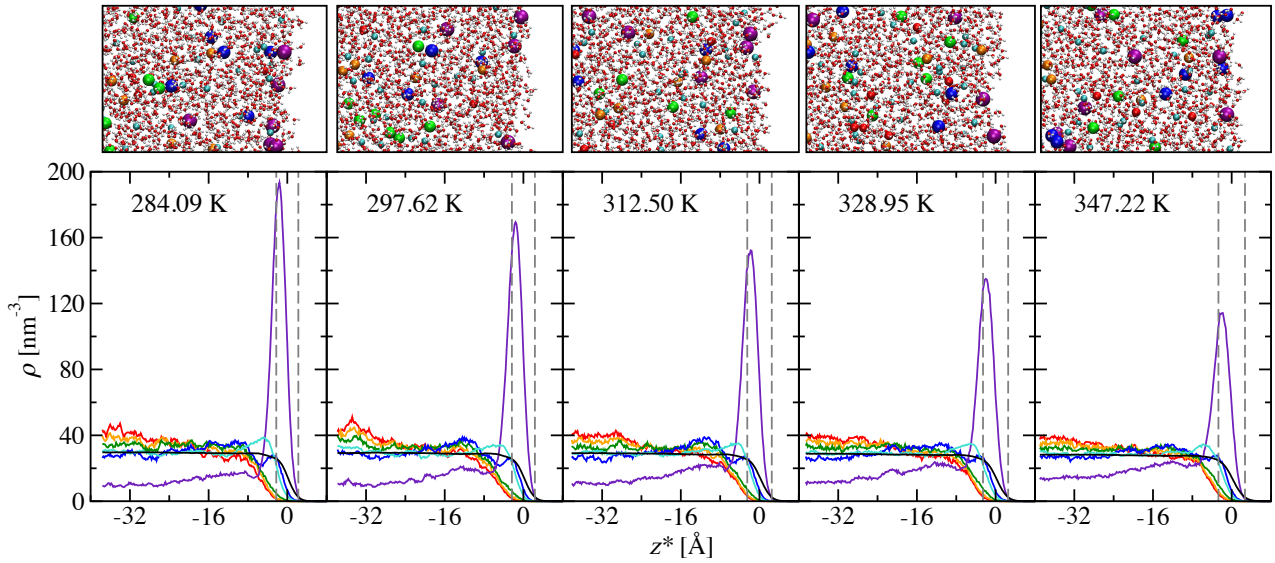

Fig. 2 Density profiles for electrolyte mixtures from 284.09 K (far left) to 347.22 K (far right). Number densities for water (black), cation (cyan), ion A (red), ion B (orange), ion C (green), ion D (blue), and ion E (purple) are shown as a function of $z^* = z - z_0$, i.e., the Gibbs dividing surface is always located at $z^* = 0$, and negative values for z^* extend into the interior of the slab. A histogram bin width of 0.2 Å is used for each profile, and the anion and cation number densities are scaled by factors of 200 and 40, respectively, to account for the differences in numbers of particles. The dashed gray lines indicate the width of the interface. Representative snapshots are also shown, oriented and scaled to match the z axis of the density profiles.

Table 2 Location of the Gibbs dividing surface, interfacial width, bulk liquid water density, and surface tension for the electrolyte mixtures

T [K]	z_0 [Å]	ξ [Å]	ρ_{liq} [kg/m^3]	γ [mN/m]
284.09 K	37.88 ± 0.02	2.04 ± 0.03	941 ± 2	55 ± 5
297.62 K	38.16 ± 0.02	2.13 ± 0.03	932 ± 2	53 ± 3
312.50 K	38.53 ± 0.02	2.27 ± 0.02	924 ± 2	51 ± 3
328.95 K	38.99 ± 0.02	2.33 ± 0.03	913 ± 2	48 ± 2
347.22 K	39.41 ± 0.02	2.46 ± 0.03	896 ± 2	46 ± 3

solvent molecules, and the density profiles are symmetrized, i.e., averaged over both interfaces. z_0 is the location of the GDS, and ξ is a measure of the interfacial width. In the mixture simulations described here, the thickness of the slab is given by $2z_0$, and the "bulk" liquid region is defined as the interior 30 Å of the slab. The results of the fitting to Equation 1 are summarised in Table 2. The data show that, as temperature increases, ρ_{liq} decreases. Correspondingly, the liquid slab expands slightly (i.e., z_0 increases), and the interface gets a bit wider (i.e., ξ goes up). All of this is expected as the solvent molecules experience increased thermal motion at the higher temperatures. The values of ρ_{liq} fall about 5% below those observed for neat water at the same temperature, and this is attributed to the presence of the ions. Especially with large ions, the volume occupied by the ions contributes to lowering the overall density for water. In our previous study, we confirmed that if the ion volume is excluded from the density calculation, the bulk density of neat water is recovered.[17]

Figure 2 shows the variation of the number densities for water and all the ions as a function z. The common reference point across all temperatures is z_0 (i.e., we are accounting for the temperature dependence of the slab thickness); negative values for $z^* = z - z_0$ indicate the relative distance below the GDS towards the bulk region of the slab. Given the variation in z_0, the interior 30 Å bulk liquid region begins at $z^* < -22.88$ Å at 284.09 K and $z^* < -24.41$ Å at 347.22 K. The most striking feature in Figure 2 is the large peak for ion E (the largest anion) at about 2 Å below the GDS but still within the interfacial width ($z^* > -\xi$). This large ion preferentially solvates into the interface and has a correspondingly low density in the bulk region. This preference persists across the temperature range. Although the height of the peak decreases by about 40% from 284 to 347 K, it still remains a significant peak. Likewise, the density for ion E in the bulk liquid region remains noticeably lower throughout all temperatures than for the other ions. In contrast, the three smaller ions (ions A-C) have negligible density in the interfacial region and a nearly monotonic increase in density until the interior of the slab is reached; trends that persist across all of the temperatures. These ions are effectively excluded from the interface and changing the temperature does not change their preferential solvation to the same extent as observed for ion E. Between these extremes is ion D, its density increases from the interior toward a broad peak at $z^* \approx -10$ Å, followed by a shallow minimum, and a smaller peak at $-\xi$. The cation density holds steady from the interior toward the surface where a small peak is found at $z^* \approx -6$ Å, i.e., the cation peak is shifted inward compared to ion E, but its location coincides with the minimum for ion D.

Within each mixture, ions D and E have the strongest preference for the interface and are blocking the other anions from occupying the surface region. We observed previously that the larger ions in a mixture can prevent smaller ions from reaching the interface, even if those smaller ions by themselves (or in a mixture with even smaller ions) would prefer to be there.[17] The density profiles here show that, as ion size increases, the ions are

able to press closer to the interface, but in this case only ions D and E have appreciable densities in the interfacial region. The result is that ions A through C form a group with very similar behavior, while ion D and ion E are both distinct from this group and distinct from each other.

Table 2 also includes values for the surface tension of these electrolyte mixtures. Salts dissolved in water, particularly small halides, will increase the surface tension of the salt solution relative to pure water. This is typically taken as an indication that the salt ions are depleted at the interface (meaning they are preferentially found below the GDS), though simulation studies have shown that it is also possible to have ions at the surface and still see an increase in surface tension due to depletion regions just below the surface.[8] The surface tension values observed here for electrolyte mixtures are very similar to neat water interfaces at similar temperatures. For example, Vega and de Miguel report 55.7 and 45.8 mN/m for 1024 TIP4P particles at 300 and 350 K, respectively, both calculated using Ewald summation for Coulomb interactions and neglecting LJ tail corrections, though with a slightly shorter cutoff (13 Å).[38] With fairly large error bars, caution is warranted in drawing firm conclusions, but the fact that our surface tension values track so closely with neat water may be attributed to the balancing effects of having a mixture of ions, some that preferentially adsorb at the interface and some that do not.

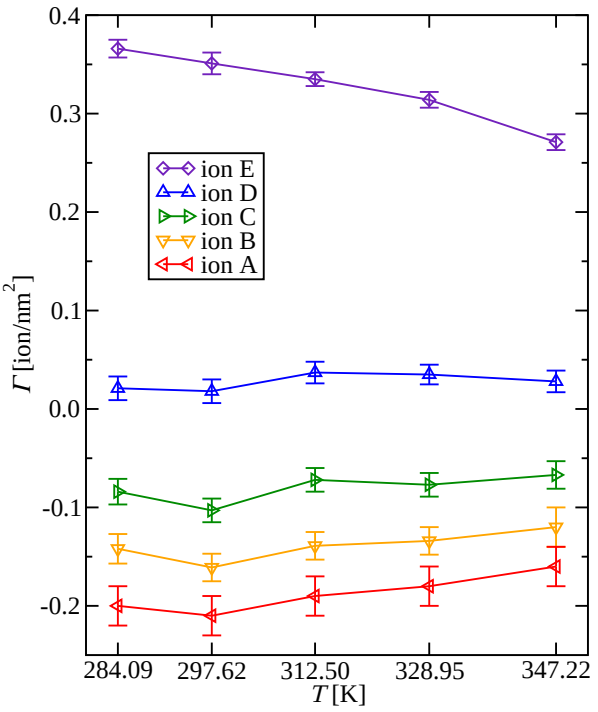

Fig. 3 Variation of surface excess with temperature. Connecting lines between data points are provided as a visual guide.

3.2 Surface Excess

According to the Gibbs adsorption isotherm model,[39] changes in the surface tension of an interface are related to changes in the surface excess of each component in the system. Surface excess for a particular component i can be calculated using the following equation

$$\Gamma_i = N_i^{\mathrm{ex}}/2A = (N_i^{\mathrm{I}} - \rho_{i,\mathrm{vap}} V_{\mathrm{vap}}^{\mathrm{I}} - \rho_{i,\mathrm{liq}} V_{\mathrm{liq}}^{\mathrm{I}})/2A \qquad (2)$$

where N_i^{ex} is the number of excess particles (i.e., the number of particles of type i in the interface box exceeding those that would be found, on average, if the system would consist only of bulk liquid and vapor regions), A is the surface area of the interface (doubled in this case because there are two symmetrized interfaces in each slab), N_i^{I} is the total number of particles of type i in the interfacial box, $\rho_{i,\mathrm{liq}}$ and $\rho_{i,\mathrm{vap}}$ are the average number densities found in the bulk liquid and vapor regions of the interfacial box, and $V_{\mathrm{vap}}^{\mathrm{I}}$ and $V_{\mathrm{liq}}^{\mathrm{I}}$ are the volumes of the liquid and vapor regions of the interfacial box, given by $2z_0A$ and $A(L_z - 2z_0)$, respectively. For all ions, $\rho_{i,\mathrm{vap}}$ is zero.

Figure 3 shows the surface excess values for all of the ions in our electrolyte mixtures, as calculated by Equation 2. Notably, the surface excess values of ions A to C are all below zero and fall relatively close together, indicating some degree of surface depletion as already observed in the density profiles. The surface excess values for ion D falls just above zero. Ion E is the most distinctive ion in our mixture with a large positive surface excess clearly separated from all the other ions. This shows that a positive surface excess can be achieved even when the (large) peak in the density profile falls below the GDS (see Figure 2). The surface excess for ion E also exhibits a noticeable decrease with increasing temperature, changing from 0.366 ± 0.009 to 0.271 ± 0.008 ion/nm^2. However, when considering the sum of the surface excess values for the anions, then Γ_{anion} is slightly negative, but very small in magnitude, and changes only from -0.039 to -0.048 ion/nm^2 as temperature increases. Similarly, Γ_{cation} is slightly negative and on average 40% larger in magnitude than for the anions. Thus, both the group of anions and the cation show negligible surface depletion in agreement with the observation that the surface tension for the electrolyte mixture is very close to that of neat water.

3.3 van't Hoff Analysis of Adsorption Thermodynamics

The van't Hoff equation relates the temperature dependence of an equilibrium constant, K, taken here as the partition constant for an ion of type i between the bulk liquid region and a region corresponding to a specific z interval, to the enthalpy change for the process (i.e., the transfer from the bulk liquid region to the specific z interval). Our simulations allow $K_{i,z}$ to be determined from the ratio of the average densities for ion i in the two regions:[40]

$$K_{i,z} = \frac{\rho_{i,z}}{\rho_{i,\mathrm{bulk}}} \qquad (3)$$

The bulk liquid region, as discussed above, is the middle 30 Å of each slab, where the ions have relatively constant number density profiles and experience bulk solvation, or at least minimal impact from the presence of the interfaces. Given our interests in this work, we then define two distinct surface regions, each 5 Å in thickness: one that is centered on the GDS (i.e., -2.5 Å $\leq z^* \leq$ 2.5 Å), and one that is centered on the location of the density

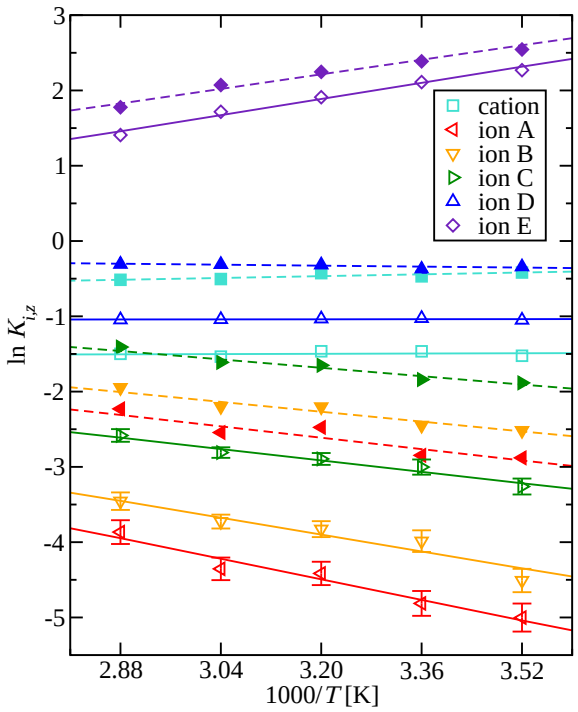

Fig. 4 van't Hoff plot for individual ions partitioning between bulk and interfacial regions. The latter are 5 Å regions, one centered on the GDS (open symbols and solid lines; -2.5 Å $\leq z^* \leq 2.5$ Å) and one centered on the location of the density maximum for ion E (filled symbols and dashed lines; -4.5 Å $\leq z^* \leq 0.5$ Å). The lines represent weighted linear least-squares fits. Error bars are only shown when larger than the symbol size.

maximum for ion E at $z^* = -2$ Å (see Figure 2, -4.5 Å $\leq z^* \leq 0.5$ Å).

From the partition constant ($K_{i,z}$), the transfer Gibbs free energy can be calculated directly:[41]

$$\Delta G_{i,\mathrm{trans}}(z,T) = -RT \ln K_{i,z} = \Delta H_{i,\mathrm{trans}}(z) - T\Delta S_{i,\mathrm{trans}}(z) \qquad (4)$$

The partition constants can also be used in the van't Hoff relationship to determine the enthalpy of transfer, $\Delta H_{i,\mathrm{trans}}(z)$, assumed to be constant over the temperature range investigated:

$$\frac{d \ln K_{i,z}}{d(1/T)} = -\frac{\Delta H_{i,\mathrm{trans}}(z)}{R} \qquad (5)$$

With $\Delta G_{i,\mathrm{trans}}(z,T)$ and $\Delta H_{i,\mathrm{trans}}(z)$ known, the entropy of transfer, $\Delta S_{i,\mathrm{trans}}(z)$, is then calculated from the second half of Equation 4.

The van't Hoff plot for ion partitioning into the two interfacial regions is shown in Figure 4. Both regions yield consistent results. Once again, we see that ions A through C fall into a group, with ions D and E showing distinctive trends. In the group of smaller anions, all have negative $\ln K_{i,z}$ values and negative slopes indicating positive (and unfavorable) $\Delta H_{i,\mathrm{trans}}(z)$. The unfavorable enthalpy experienced by these ions moving from the bulk to the surface dictates a preference for bulk solvation in the electrolyte mixture. Ion D has an essentially flat van't Hoff line, meaning $\Delta H_{\mathrm{D,trans}}(z)$ is close to zero, and the $\ln K_{\mathrm{D},z}$ values for the two interfacial regions are small in magnitude, so it seems that ion D is not experiencing any real preferences for either bulk or surface solvation. The peak in the density profile for ion D is found at $z^* \approx -10$ Å, i.e., well below that of ion E, and this explains why ion D exhibits both a positive surface excess, but unfavorable partitioning into the interfacial regions. In contrast, ion E does have a clear preference for surface adsorption. For this ion, the van't Hoff plot shows a positive slope and overall positive $\ln K_{\mathrm{E},z}$ values. The positive slope is associated with a negative (favorable) $\Delta H_{\mathrm{E,trans}}(z)$. The cation yields similar van't Hoff data as ion D with only small negative $\ln K_{\mathrm{cation},z}$ values that do not depend much on temperature. In this electrolyte mixture, ion E is the only ion that can be said to have a strong preference for interfacial adsorption, and that preference is, at least in part, determined by the favorable enthalpy that comes with moving this large ion into the interface. A note of caution is warranted, however, because the presence of slight curvature in the van't Hoff plot for ion E is indicative of heat capacity effects which make the van't Hoff analysis less reliable.[31] Comparing the data for the two surface regions, the region centered on the density maximum for ion E and shifted by 2 Å toward the bulk exhibits $\ln K_{i,z}$ values that are shifted upward (and correspondingly, $\Delta G_{i,\mathrm{trans}}(z,T)$ values are smaller). This upward shift in $\ln K_{i,z}$ is most pronounced for ion A with the strongest preference for surface depletion.

Table 3 Gibbs free energies, enthalpies, and entropies of transfer for ions between the bulk liquid and the two surface regions at $T = 312.50$ K

Ion	$\Delta G_{\mathrm{trans}}$ [kJ/mol]	$\Delta H_{\mathrm{trans}}$ [kJ/mol]	$\Delta S_{\mathrm{trans}}$ [J/K mol]
	interface region ($z = -2.5$ to 2.5 Å)		
A	11.5 ± 0.4	14.2 ± 0.9	9 ± 3
B	9.9 ± 0.3	11.7 ± 0.9	5 ± 3
C	7.5 ± 0.2	7.9 ± 0.4	1 ± 2
D	2.7 ± 0.2	-0.06 ± 0.07	-8.6 ± 0.6
E	-4.96 ± 0.11	-11.1 ± 0.4	-19.5 ± 1.3
cation	3.8 ± 0.2	-0.2 ± 0.3	-12.8 ± 1.0
	peak region ($z = -4.5$ to 0.5 Å)		
A	6.43 ± 0.04	7.9 ± 0.8	4 ± 3
B	5.72 ± 0.05	6.8 ± 0.5	4 ± 2
C	4.29 ± 0.05	5.8 ± 0.4	5 ± 1
D	0.82 ± 0.07	0.67 ± 0.14	-0.6 ± 0.6
E	-5.84 ± 0.07	-10.1 ± 0.5	-13 ± 2
cation	1.1 ± 0.4	-1.3 ± 0.2	-7.7 ± 0.6

Table 3 provides the thermodynamic data at the intermediate temperature from the van't Hoff analysis. These data allow one to elucidate the thermodynamic driving forces for the observed ion distribution. Ions A through C are depleted at the interface because of a very unfavorable $\Delta H_{i,\mathrm{trans}}(z)$. Although $\Delta S_{i,\mathrm{trans}}(z)$ values for these ions are positive, they are not favorable enough to overcome the unfavorable $\Delta H_{i,\mathrm{trans}}(z)$. Here we can attribute the large unfavorable $\Delta H_{i,\mathrm{trans}}(z)$ at the interface to the conventional explanation, namely that these small ions would lose favorable interactions with water molecules through a partial loss of their tight hydration shell if they were to move into the interface ($\Delta H_{i,\mathrm{trans}}(z) > 0$); at the same time, the entropic penalty for cavity formation would be diminished if the ions were to leave the bulk ($\Delta S_{i,\mathrm{trans}}(z) > 0$). For ions D and E, there is a change in sign for both $\Delta H_{i,\mathrm{trans}}(z)$ and $\Delta S_{i,\mathrm{trans}}(z)$. As these ions move to the interface, $\Delta H_{i,\mathrm{trans}}(z)$ is negative, which others have attributed to the recovery of favorable water-water interactions as these large

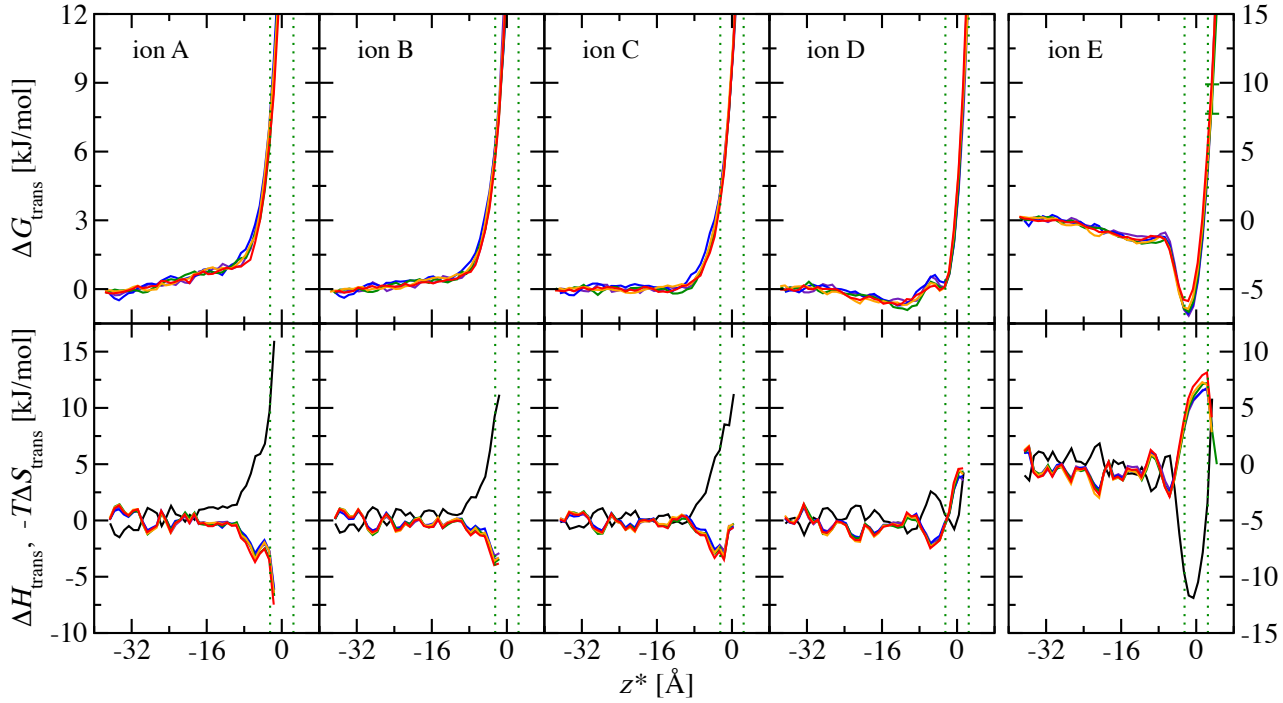

Fig. 5 Enthalpy, entropy, and Gibbs free energy of transfer profiles for individual anions. $\Delta G_{i,\mathrm{trans}}(z)$ and $-T\Delta S_{i,\mathrm{trans}}(z)$ are shown for all five temperatures: 284.09 K (purple), 297.62 K (blue), 312.50 K (green), 328.95 K (orange), and 347.22 K (red). $\Delta H_{i,\mathrm{trans}}(z)$ is shown in black. A different scale is used for ion E. Due to lack of sufficient statistics, $\Delta H_{i,\mathrm{trans}}(z)$ and $-T\Delta S_{i,\mathrm{trans}}(z)$ are only shown when $\Delta G_{i,\mathrm{trans}}(z) < 12$ kJ/mol. Error bars are shown only when larger than 1 kJ/mol for $\Delta G_{i,\mathrm{trans}}(z)$ and larger than 2 kJ/mol for $\Delta H_{i,\mathrm{trans}}(z)$ and $-T\Delta S_{i,\mathrm{trans}}(z)$. The green dotted lines indicate the width of the interface at the intermediate temperature.

ions are partially desolvated (loss of favorable ion-water interactions) when moving toward the surface.[4,11,21–24,28] The strength of the ion-water interactions diminishes with increasing size of the anion, and this may help to explain why the effect is most pronounced for ion E. Interestingly, we find that $\Delta S_{i,\mathrm{trans}}(z)$ for these ions moving to the interface is also negative (i.e., unfavorable). Netz and Horinek[4] carried out potential of mean force calculations for a non-polarizable iodide model over an extended temperature range from 260 to 380 K and found that the minimum near the interface becomes more shallow with increasing temperature described by $\Delta S_{\mathrm{trans}} = -17.8$ J/K mol; i.e., a value that is consistent with $\Delta S_{\mathrm{E,trans}}(z)$ for the peak region.

The observation that $\Delta S_{i,\mathrm{trans}}(z)$ for interfacial adsorption changes from a positive value for ion A to a negative value for ion E runs contrary to the explanation based on the entropic cost of cavity formation that yields an increasing entropic gain with increasing ion volume. While water molecules are gaining entropy from the collapse of a cavity for the ion, there are more complex interactions also at work that may lead to a net loss of entropy when this large ion moves to the interface. One possibility is that ions at the interface restrict natural capillary waves that characterize these interfaces,[21,24] while more recent studies indicate changes in direct ion-water interactions to be responsible (with cancelling enthalpic and entropic terms from solvent-induced changes in water-water interactions).[26–28] For an ionic mixture, there is also the entropic cost for demixing the anions to allow for preferential adsorption of the larger anion, and it is plausible that the ion distribution in the mixture should become more uniform with increasing temperature. However, we again want to highlight the curvature observed in the van't Hoff plot for ion E (see Figure 4). The downward curvature (or decreasing slope) may indicate a decrease in magnitude of $\Delta H_{\mathrm{E,trans}}(z)$ as temperature increases, i.e., a positive heat capacity of transfer, because the favorable water-water interactions gained upon partial desolvation become smaller in magnitude. Since transfer heat capacity and $-\Delta S_{i,\mathrm{trans}}(z)$ similarly effect the temperature dependence of $\ln K_{i,z}$, they could only be separated by a calorimetric measurement. We have previously investigated heat capacity effects for self-solvation because the entropy of transfer can be calculated for this case with great precision,[31] but this approach cannot be applied for the electrolyte mixture because the ion solvation is only a relatively small part of the total energy.

To obtain a more granular perspective on the contributions from $\Delta H_{i,\mathrm{trans}}(z)$ and $\Delta S_{i,\mathrm{trans}}(z)$ across the entire liquid slab, the values from the density profiles are grouped into 1.0 Å regions, and the van't Hoff analysis is extended to these very small regions (see Figure 5). Of course, statistical uncertainties increase significantly when reducing the analysis region by a factor of 5, and the 30 Å central region is still used to calculate $\rho_{i,\mathrm{liq}}$ in Equation 3. Ions A through C, which are to varying extent excluded from the interface, show similar $\Delta G_{i,\mathrm{trans}}(z)$ profiles, with a modest positive slope for small z^* values, a sharp bend at $z^* \approx -8$ Å, and a very steep rise as the GDS is approached. For the initial part ($z^* < -8$ Å), the positive slope diminishes as the ion size increases, and this part is nearly flat for ion C. The profile for ion D shows some similarity to the smaller anions, but exhibits some additional features.

The slope for $\Delta G_{\mathrm{D,trans}}(z)$ changes to slightly negative for $z^* > -24$ Å, reaching a minimum at $z^* \approx -12$ Å, then rises until $z^* \approx -6$ Å, followed by a flat part, and finally the steep rise as $z^* > -2$ Å. For ion E, the change toward negative $\Delta G_{\mathrm{E,trans}}(z)$ values also starts at $z^* \approx -24$ Å, but the slope is much larger in magnitude than for ion D. For ion E, there is a shallow local minimum at $z^* \approx -12$ Å. Whereas the global minimum in $\Delta G_{\mathrm{D,trans}}(z)$ is only about -1 kJ/mol for ion D, ion E exhibits a comparatively deep minimum near -2 Å that ranges from -7.0 kJ/mol at 284.09 K to -6.0 kJ/mol at 347.22 K.

The bottom half of Figure 5 shows z profiles of both $\Delta H_{i,\mathrm{trans}}(z)$ and $\Delta S_{i,\mathrm{trans}}(z)$. Again the trends show similarities for the group of ions A through C, and support that $\Delta H_{i,\mathrm{trans}}(z)$ is the dominant factor in determining the $\Delta G_{i,\mathrm{trans}}(z)$ and a given ion's relative preference for the surface or the bulk liquid. For ions A through C, $\Delta H_{i,\mathrm{trans}}(z)$ values become large and positive (unfavorable) well below the GDS ($z^* > -8$ Å). For ion D, $\Delta H_{\mathrm{D,trans}}(z) \approx 0$ kJ/mol at the GDS, then rises steeply as more of the solvation shell is lost for larger z^* values. In contrast, there is a deep minimum in $\Delta H_{\mathrm{E,trans}}(z) \approx -12$ kJ/mol for ion E at $z^* > -2$ Å. For ion E, $\Delta H_{\mathrm{E,trans}}(z)$ becomes positive only for $z^* > \xi$, i.e., when leaving the interfacial region.

In general, the $T\Delta S_{i,\mathrm{trans}}(z)$ values are smaller in magnitude than the $\Delta H_{i,\mathrm{trans}}(z)$ values at the same location; and for most of the z range, $-T\Delta S_{i,\mathrm{trans}}(z)$ and $\Delta H_{i,\mathrm{trans}}(z)$ have opposite sign, i.e., there is enthalpy-entropy compensation. For ion A, $\Delta S_{\mathrm{A,trans}}(z)$ becomes favorable for $z^* > -8$ Å, and the negative slope in $-T\Delta S_{\mathrm{A,trans}}(z)$ increases until the GDS is reached. Beyond the GDS, the number densities become too small (more than a factor of 100 smaller than $\rho_{i,\mathrm{liq}}$, i.e. $\Delta G_{i,\mathrm{trans}}(z) > 12$ kJ/mol) and do not anymore allow for a decomposition of $\Delta G_{i,\mathrm{trans}}(z)$. For ion B, $\Delta S_{\mathrm{B,trans}}(z)$ also favors interfacial adsorption, but the negative slope becomes smaller as the GDS is approached indicating the existence of a minimum in $-T\Delta S_{i,\mathrm{trans}}(z)$ near the GDS. As possible explanation for this change in slope could be that an ion location above the GDS would require formation of an entropically disfavored water "neck" to keep some of the ion's solvation. For ion C, this minimum in $-T\Delta S_{\mathrm{C,trans}}(z)$ is more pronounced. Again, ions D and E show features quite distinct from the three smaller ions. For ion D, the minimum in $-T\Delta S_{\mathrm{D,trans}}(z)$ shifts further inward and is now found at $z^* \approx -5$ Å, while a maximum is found just above the GDS, and $\Delta S_{\mathrm{D,trans}}(z)$ becomes favorable for $z^* > -\xi$. For ion E, we do not observe a local minimum in $-T\Delta S_{\mathrm{E,trans}}(z)$ below the interfacial region, and partitioning into the interfacial region is associated with a positive $-T\Delta S_{\mathrm{E,trans}}(z)$. As for ion D, there is indication that further desolvation beyond $z^* > \xi$ would become entropically favorable for ion E. The combination of negative $\Delta H_{\mathrm{E,trans}}(z)$ and negative $\Delta S_{\mathrm{E,trans}}(z)$ in the interfacial region is consistent with what others have observed in experiment, simulation, and theory.[11,21–24,28] The $\Delta H_{\mathrm{E,trans}}(z)$ and $-T\Delta S_{\mathrm{E,trans}}(z)$ profiles for ions D and E bear remarkable similarities in locations of changes in slope and of extrema and their magnitudes with recent works on non-polarizable chloride[25] and iodide,[28] respectively.

3.4 Ion Pairing

Since the (total) ion to water molar ratio of 1:21 (equivalent to a total salt concentration of 1.3 mol/kg) used in our study is relatively high, ion pairing may also play a role in the adsorption thermodynamics. To this extent, we are most interested in the profiles of the anion-cation coordination numbers as function of z^* (see Figure 6). Analysis of the anion-cation radial distribution functions (averaged over the entire simulation box) yields two distinct peaks for contact and solvent-separated ion pairs (CIP and SSIP, respectively) with the positions of the first and second minima being remarkedly independent of temperature. The positions of these minima are given in Figure 6 and can be used as distance cut-offs to define CIP and SSIP. To obtain the ion-pairing depth profile, we collect anions in 1 Å wide z^* regions and calculate the anion-cation number integral out to the CIP cut-off and the incremental number integral from CIP to SSIP cut-off to obtain the corresponding coordination numbers, $N_{i,\mathrm{CIP}}$ and $N_{i,\mathrm{SSIP}}$, respectively. Given the relatively small number of anions in a given z^* region, our statistics are insufficient to consider an angular component near the interface or to compute the barrier separating CIP and SSIP as recently done by Dang and Schenter in the calculation of potentials of mean force parallel and perpenticular to the interface.[42]

As for many of the other properties, the three smaller anions yield similar anion-cation coordination number profiles (see Figure 6). For $N_{i,\mathrm{CIP}}$, there is a clear increase with increasing z^* when moving from the bulk liquid toward the interface with a peak at $z^* \approx -5$ Å. In contrast, $N_{i,\mathrm{CIP}}(z)$ is nearly flat for ions D and E for $z^* < -12$ Å, followed by a peak at $z^* \approx -8$ Å and a shoulder at $z^* \approx 0$ Å. The reason for the shoulder is the depletion of cations near the GDS (see Figure 2). Overall, the indermediate-size ions yield more contact ion pairing than observed for ions A and E. The finding of a higher propensity for CIP formation near the interface is consistent with other recent simulation studies.[9,12,25,42] When considering SSIPs, then the profiles for all five ion types are quite similar with a small increase in $N_{i,\mathrm{SSIP}}$ and a more pronounced shoulder for ion E. With regard to temperature effects, we find an increase in CIP formation near the interface for ion A, but a decrease for ion E. This change in the propensity for interfacial ion pairing may also contribute to the change in sign of $\Delta S_{i,\mathrm{trans}}(z)$ for interfacial adsorption.

4 Conclusions

Simulations of electrolyte mixtures demonstrate that different ions experience preferences for surface or bulk solvation for different reasons. Our simulations reveal three different ways that ions partition into the interface, with three different thermodynamic explanations. One type of ion, represented here by the smallest ions (A through C with $\sigma \leq 5.1$ Å), exhibits behavior consistent with conventional view points on ion solvation, i.e., preferring bulk solvation and showing negative surface excess on the basis of unfavorable $\Delta H_{i,\mathrm{trans}}$ because of loss of favorable ion-water interactions that overwhelms the favorable entropic gain of loosing the complete cavity in the bulk liquid. Another type, ion D ($\sigma = 5.7$ Å), does not exhibit a strong preference for either bulk or surface solvation and possesses only small enthalpies and

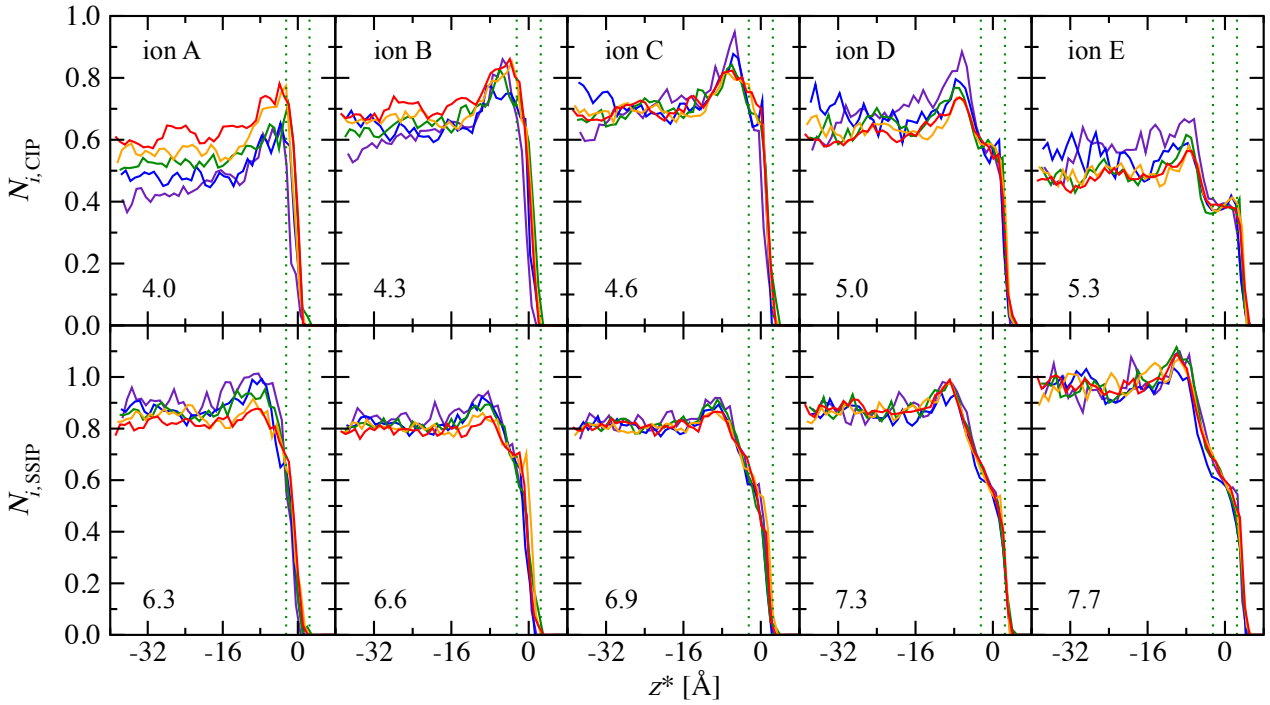

Fig. 6 Contact-ion-pair (top) and solvent-separated-ion-pair coordination number profiles for individual anions. $N_{i,\mathrm{CIP}}(z)$ and $N_{i,\mathrm{SSIP}}(z)$ are shown for all five temperatures: 284.09 K (purple), 297.62 K (blue), 312.50 K (green), 328.95 K (orange), and 347.22 K (red). The green dotted lines indicate the width of the interface at the intermediate temperature. The numbers below the ion label indicate the anion-specific values of the spherical cut-offs used for the determination of contact and solvent-separated ion pairs.

entropies of transfer into the interface. The largest ion in the mixture, ion E ($\sigma = 6.4$ Å), strongly prefers surface solvation and unexpectedly exhibits favorable enthalpies of transfer into the interface with smaller unfavorable entropies–likely because the favorable water-water interactions gained upon desolvation are larger in magnitude than the loss of ion-water interactions. Clearly, the presence of other ions in a mixture may further enhance or diminish tendencies for interfacial adsorption that would occur when only one type of ion is present in the solution. For example, without the presence of ion E, we expect that ion D would show a stronger preference for surface adsorption. The ion types at the extrema of the size range, ions A and E, are found to be most affected by changes in the temperature with opposite signs for the entropy of interfacial adsorption, the change in surface excess, and the propensity for contact ion pairing at the interface.

Conflicts of interest

There are no conflicts to declare.

Acknowledgements

Financial support from the National Science Foundation (CBET-1159837 and RUI-1159731) and the Industrial Partnership for Research in Interfacial & Materials Engineering at the University of Minnesota is gratefully acknowledged.

Notes and references

1 P. B. Petersen and R. J. Saykally, *Annu. Rev. Phys. Chem.*, 2006, **57**, 333–364.

2 D. J. Tobias, A. C. Stern, M. D. Baer, Y. Levin and C. J. Mundy, *Annu. Rev. Phys. Chem.*, 2013, **64**, 339–59.

3 L. Onsager and N. N. T. Samaras, *J. Chem. Phys.*, 1934, **2**, 528–536.

4 R. R. Netz and D. Horinek, *Annu. Rev. Phys. Chem.*, 2012, **63**, 401–4018.

5 E. M. Knipping, M. J. Lakin, K. L. Foster, P. Jungwirth, D. J. Tobias, R. B. Gerber, D. Dabdub and B. J. Finlayson-Pitts, *Science*, 2000, **288**, 301–306.

6 L. Perera and M. L. Berkowitz, *J. Chem. Phys.*, 1991, **95**, 1954.

7 L. X. Dang and D. E. Smith, *J. Chem. Phys.*, 1993, **99**, 6950–6956.

8 P. Jungwirth and D. J. Tobias, *J. Phys. Chem. B*, 2002, **106**, 6361–6373.

9 J. D. Smith and S. W. Rick, *Condens. Matt. Phys.*, 2016, **19**, 1–10.

10 M. D. Baer and C. J. Mundy, *J. Phys. Chem. Lett.*, 2011, **2**, 1088–1093.

11 A. C. Stern, M. D. Baer, C. J. Mundy and D. J. Tobias, *J. Chem. Phys.*, 2013, **138**, 114709.

12 C. D. Daub, V. Hänninen and L. Halonen, *J. Phys. Chem. B*, 2019, **123**, 729–737.

13 P. Jungwirth and D. J. Tobias, *Chem. Rev. (Washington, DC, U. S.)*, 2006, **106**, 1259–1281.

14 D. Horinek, A. Herz, L. Vrbka, F. Sedlmeier, S. I. Mamatkulov and R. R. Netz, *Chem. Phys. Lett.*, 2009, **479**, 173–183.

15 J. Noah-Vanhoucke and P. L. Geissler, *Proc. Natl. Acad. Sci. U. S. A.*, 2009, **106**, 15125–15130.

16 D. J. V. A. dos Santos, F. Müller-Plathe and V. C. Weiss, *J Phys Chem C*, 2008, **112**, 19431–19442.
17 B. L. Eggimann and J. I. Siepmann, *J. Phys. Chem. C*, 2008, **112**, 210–218.
18 G. L. Warren and S. Patel, *J. Phys. Chem. C*, 2008, **112**, 7455–7467.
19 J. Cheng and M. Sprik, *Phys. Rev. B*, 2010, **82**, 081406.
20 E. S. Boek and M. Sprik, *J. Phys. Chem. B*, 2003, **107**, 3251–3256.
21 C. Caleman, J. S. Hub, P. J. van Maaren and D. van der Spoel, *Proc. Natl. Acad. Sci. U. S. A.*, 2011, **108**, 6838–6842.
22 D. E. Otten, P. R. Shaffer, P. L. Geissler and R. J. Saykally, *Proc. Natl. Acad. Sci. U. S. A.*, 2012, **109**, 701–705.
23 X. Li and G. C. Schatz, *J. Phys. Chem. Lett.*, 2013, **4**, 2885–2889.
24 S. Ou and S. Patel, *J. Phys. Chem. B*, 2013, **117**, 6512–6523.
25 V. Venkateshwaran, S. Vembanur and S. Garde, *Proc. Natl. Acad. Sci. U. S. A.*, 2014, **111**, 8729–8734.
26 D. Ben-Amotz, *J. Phys.: Condens. Matter*, 2016, **28**, 414013.
27 K. Rane and N. F. A. van der Vegt, *J. Phys. Chem. B*, 2016, **120**, 9697–9707.
28 P. K. Wise and D. Ben-Amotz, *J. Phys. Chem. B*, 2018, **122**, 3447–3453.
29 Y. Wang, S. Sinha, P. R. Desai, H. Jing and S. Das, *J. Am. Chem. Soc.*, 2018, **140**, 12853–12861.
30 N. Ottosson, J. Heyda, E. Wernersson, W. Pokapanich, S. Svensson, B. Winter, G. Öhrwall, P. Jungwirth and O. Björneholm, *Phys. Chem. Chem. Phys.*, 2010, **12**, 10693–10700.
31 C. D. Wick, J. I. Siepmann and M. R. Schure, *J. Phys. Chem. B*, 2003, **107**, 10623–10627.
32 W. L. Jorgensen, J. Chandrasekhar, J. D. Madura, R. W. Impey and M. L. Klein, *J. Chem. Phys.*, 1983, **79**, 926–935.
33 J. I. Siepmann and D. Frenkel, *Mol. Phys.*, 1992, **75**, 59–70.
34 G. C. A. M. Mooij, D. Frenkel and B. Smit, *J. Phys.: Condens. Matter*, 1992, **4**, L255–L259.
35 T. J. H. Vlugt, M. G. Martin, B. Smit, J. I. Siepmannm and R. Krishna, *Mol. Phys.*, 1998, **94**, 727–733.
36 A. Z. Panagiotopoulos, *Mol. Phys.*, 1987, **61**, 813–826.
37 A. Z. Panagiotopoulos, N. Quirke, M. Stapleton and D. J. Tildesley, *Mol. Phys.*, 1988, **63**, 527–545.
38 C. Vega and E. de Miguel, *J. Chem. Phys.*, 2007, **126**, 154707.
39 A. Zangwill, *Physics at Surfaces*, Cambridge University Press, Cambridge, 1988.
40 J. L. Rafferty, L. Zhang, J. I. Siepmann and M. R. Schure, *Anal. Chem.*, 2007, **79**, 6551–6558.
41 A. Ben-Naim, *Molecular Theory of Solutions*, Oxford University Press, Oxford, 2006.
42 L. X. Dang and G. K. Schenter, *J. Chem. Phys.*, 2018, **148**, 222820.